JOURNAL OF AIRCRAFT
Vol. 36, No. 6, November–December 1999

Effects of Freestream Turbulence on Wing-Surface Flow and Aerodynamic Performance

Rong F. Huang* and Han W. Lee†
National Taiwan University of Science and Technology, Taipei 106, Taiwan, Republic of China

The effects of freestream turbulence intensity on the surface-flow characteristics, including separation, bubble, leading-edge bubble, turbulent separation, and three-dimensional flow, as well as the corresponding aerodynamic performance, including lift, drag, and stall, of a cantilever NACA 0012 wing model have been studied in a wind tunnel. Different wire-mesh screens were placed between the nozzle and test section to produce various freestream turbulence intensities. The characteristic regimes of surface flow were identified by using the surface-oil flow technique. The aerodynamic lift and drag were measured with a PC-based force/moment sensing system. The variations of lift and drag were found to be closely related to the behavior of surface flow. The freestream turbulence significantly affects the surface flow and aerodynamic performance. The surface flow and lift/drag at low freestream turbulence are apparently different from that at large freestream turbulence intensity. The influence is drastic when turbulence intensities are smaller than about 0.45%, whereas it becomes insignificant when turbulence intensities are greater than 0.45%. Details of the influences are discussed and illustrated.

Nomenclature

b	= span of wing, 30 cm
C_D	= drag coefficient, D/qbc
C_L	= lift coefficient, L/qbc
$C_{L,\max}$	= maximum lift coefficient prior to stall
c	= chord length of wing, 6 cm
D	= drag force, measured by balance in freestream direction
L	= lift force, measured by balance in cross freestream direction
q	= dynamic pressure of freestream, $\frac{1}{2}\rho_w u_w^2$
Re_c	= Reynolds number based on chord length of wing
T	= nominal freestream turbulence intensity, root mean square of velocity fluctuation/time-average velocity
u_w	= freestream velocity in wind-tunnel test section
X	= normalized streamwise coordinate, x/c
X_b	= normalized chordwise length of separation bubble, x_b/c
X_r	= normalized streamwise location of reattachment point of separated boundary layer on suction surface of wing, x_r/c
X_s	= normalized streamwise location of separation point of boundary layer on suction surface of wing, x_s/c
x	= streamwise coordinate, originated from leading edge of wing
x_b	= chordwise length of separation bubble
x_r	= streamwise location of reattachment point of separated boundary layer on suction surface of wing
x_s	= streamwise location of separation point of boundary layer on suction surface of wing
Y	= normalized spanwise coordinate, y/c
y	= spanwise coordinate, originated from leading edge of wing on root plane
α	= angle of attack
α_{stall}	= angle of attack at stall
ρ_w	= density of air

Received 6 December 1998; revision received 3 May 1999; accepted for publication 10 May 1999.

*Professor, Department of Mechanical Engineering, 43 Keelung Road, Sec. 4. Member AIAA.

†Graduate Student, Department of Mechanical Engineering, 43 Keelung Road, Sec. 4.

Introduction

As a lifting surface, the wing is the quintessence of flight vehicles. Carmichael's encyclopedic report[1] reviewed the known theoretical and experimental results of various airfoils spanning the chord Reynolds numbers from 10^2 to 10^9. In the range $10^2 < Re_c < 10^4$, which occurs on the insects and small model airplanes, the low aerodynamic efficiency caused by the strong and persistent laminar flow on the wing surface is essential. The light aircraft, jet transports, airships, etc., which usually have high aerodynamic performance caused by the fully turbulent behavior of boundary layer on the wing surface are found in the range $10^6 < Re_c < 10^9$. Flying animals, large model airplanes, man-carrying hang gliders, human-powered aircraft, remotely piloted vehicles (RPVs), etc., fall in the category of $10^4 < Re_c < 10^6$. In this range the aerodynamic performance of the lifting surface is low at $Re_c < 10^5$ and significantly improved at $Re_c > 10^5$. The drastic improvement in the lift/drag ratio is caused by the complex variations in the surface-flow regime over the wing.

The variations of surface flow and aerodynamic loads of a wing at Reynolds numbers in the range of $10^4 \sim 10^6$ have been studied by many investigators. Crabtree[2] studied the formation of short and long laminar separation bubbles on thin airfoils at incidence. Of the two types of separation bubbles, Crabtree showed that the long one was more significant because of its strong effect on the aerodynamic characteristics, whereas the short one should be considered in its capacity as an agent for initiating a turbulent boundary layer. Ward[3] noted that the bubble behavior might be related to the boundary-layer transition process. Most of the studies of low-Reynolds-number airfoil during the 1980s were focused on the behavior of the surface flow because of its significant influence on aerodynamic performance. For example, the reports of Refs. 4–12 were sited frequently in the literature. The general behavior of the laminar separation, transition, reattachment, etc., on the low-Reynolds-number wings were reviewed by Lissaman.[13] The laminar boundary layer, extending from the stagnation point over the leading edge, separates downstream at the point of minimum pressure under certain flow conditions and wing configurations. Transition to turbulent flow occurs in the free shear layer a short distance downstream from the separation point. The flow then reattaches to the wing surface, with a turbulent boundary layer extending from the reattachment point to the trailing edge. A bubble is found between the separation and reattachment points once the boundary layer reattaches. At low-chord Reynolds numbers and angles of attack, the bubble generally extends over a large portion of the chord length and significantly changes the

pressure distribution by tremendously altering the shape of the outer potential stream flow. The aerodynamic performance thus is significantly changed. Huang et al.[14] noted the variations of aerodynamic performance because of the change of surface-flow characteristics at different Reynolds numbers. Hence, most of the control methods currently used for low-speed airfoil aerodynamics, including suction, blowing, shaping, heating, cooling, wave cancellation, turbulators, acoustics, etc., reviewed by Gad-el-Hak[15] were focused on the modulation of the behavior of surface flow.

The appearances of surface flow reported in the literature were usually performed in different ranges of freestream turbulence and surface roughness. Hillier and Cherry[16] and Kiya and Sasaki[17] studied the influence of the freestream turbulence on the separation bubble along the side of a blunt plate with right-angled corners. The bubble length, length scale of vortices in the reattaching zone, and suction-peak pressure were correlated fairly well with the turbulence intensity outside the shear layer near the separation point. The effects of freestream turbulence on lift and drag performance of a Lissaman 7769 airfoil were presented by Mueller et al.[18] The hysteresis characteristics of the lift and drag coefficients were observed at 0.10% freestream disturbance intensity. The hysteresis loop, however, disappeared as the freestream turbulence intensity was increased to 0.30%. They argued that surface roughness could also produce results identical to those achieved with freestream disturbances. The disappearance of the hysteresis loop of aerodynamic lift and drag coefficients at high freestream turbulence intensity be related to the change of surface-flow pattern. The surface flow, however, subject to the change in freestream turbulence was not reported. In this paper the experimental results of surface-flow characteristics and aerodynamic loads of an NACA 0012 wing model at various freestream disturbances are presented.

Experimental Setup

The experiments were performed in a Göttingen-type[19] (closed-return) wind tunnel as shown in Fig. 1. The size of the test section was $60 \times 60 \times 120$ cm. The lower and upper limits of the tunnel velocity were 0.7 and 56 m/s, respectively. The freestream turbulence intensity was about 0.2% within the normal operating range 5–40 m/s. To generate different turbulence intensities in the test section, wire meshes of different mesh densities and wire diameters were placed between the nozzle outlet and the test section. There were five sets of freestream turbulence intensities employed in the study, as shown in Fig. 2. The screen number, mesh density, wire diameter, and nominal freestream turbulence intensity are listed on the plot. The nominal turbulence intensities, 0.20, 0.40, 0.45, 0.50, and 0.65%, were used in the following context. The turbulence intensity was measured with a hot-wire anemometer. To digitize the output signal of the hot-wire anemometer, the sampling rate and elapsed time of the data acquisition system were set at 16,000 samples/s and 2 s, respectively. Each record length thus had 32,000 samples. No

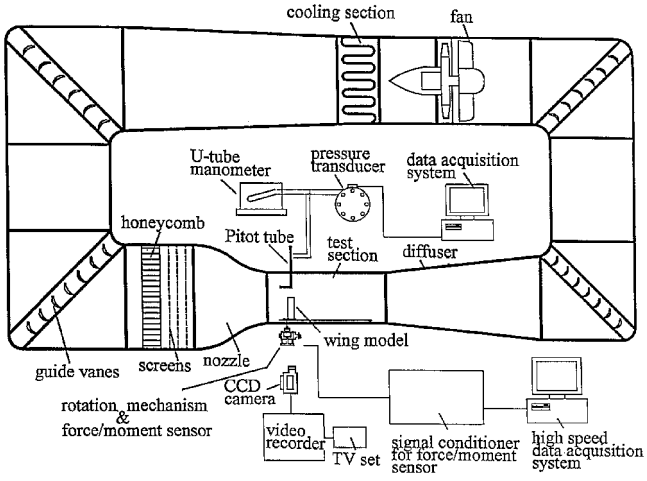

Fig. 1 Experimental setup.

Screen I.D. #	Mesh Density (meshes/cm)	Wire Diameter (mm)	Norminal Free-Stream Turbulence Intensity (T)
no screen			0.20%
#24	9.45	0.25	0.40%
#20	7.87	0.25	0.45%
#18	7.09	0.35	0.50%
#16	6.30	0.40	0.65%

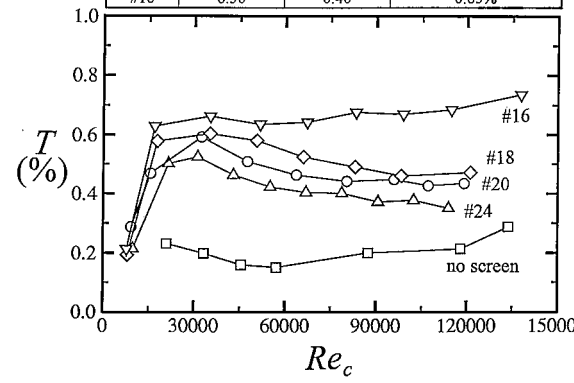

Fig. 2 Freestream turbulence intensities produced by various mesh screens.

particular peaks were found in the power spectral density function of the screen-generated turbulence so that the speculation about the synchronization of the turbulent eddies with the free shear layer that forms above the bubble was isolated. During the experiments, the average velocity of the approaching flow was determined either by using a pitot-static tube in the normal velocity range or by a calibrated hot-wire anemometer in the low-speed range. An aluminum plate with sharp leading and trailing edges was placed 5 cm above the floor of the test section for control of the boundary-layer thickness.

The rectangular wing model was made of stainless steel. The profile of the cross section was NACA 0012. A chord length of 6 cm and span of 30 cm provided an aspect ratio of 5. The wing model protruded vertically through the aluminum floor of the test section and the boundary-layer thickness control plate. The leading edge of the wing model was placed at $4.2c$ (about 200 mesh sizes) downstream from the fine-wire mesh screen so that the flow approaching the wing model is beyond the establishment and initial decay periods of the grid turbulence.

The wing model was mounted on a JR^3 Universal Force-Moment System. The assembly of wing model and balance was mounted on a rotary support. The rotary support had a resolution of 0.012 deg. The JR^3 balance had a monolithic six-degree-of-freedom force sensor. The output electronic signals of the sensor were sampled by a PC-based high-speed data acquisition system.

The surface-oil flow technique as described by Huang and Lin[20] was employed to detect the variation in flow modes. Mineral oil mixed with a small amount of blue dye powder was blush coated on the suction surface of the wing model. The dark traces on the wing surface are located where the massive dyed oil accumulated. The flow direction on the suction surface was observed in situ from the trace of oil flow motion. The positions of separation and reattachment of the boundary layer on the suction surface of the wing were taken from the recorded video images of the surface-oil flow patterns.

The accuracy of the measurement of freestream velocity was affected primarily by the alignment of the pitot tube and calibration of pressure transducer. With the help of an on-line micropressure calibration system and careful alignment of pitot tube, the uncertainty in the freestream velocity was estimated to be as large as 3% of reading. The accuracy of the angle of attack was controlled within 0.5% of reading. The uncertainty in separation location was estimated to be less than 3% of chord length. The uncertainty in reattachment location was less than 4% of chord length. The largest uncertainty in C_L is at near zero lift, i.e., at low angles of attack. It was estimated to be within 3% of reading. The largest uncertainty in C_D appears at zero angle of attack, where the drag is a minimum, and was estimated to be about 4% of reading.

Results and Discussion

Typical Surface-Flow Patterns

The typical hand sketches showing the patterns of surface-oil flow on the suction surface of the NACA 0012 wing model at $T = 0.2\%$ at various angles of attack are shown in Fig. 3. The bold lines delineate the separation or reattaching lines, whereas the thin lines with arrow heads indicate the paths and directions of oil flow on the suction surface. The hand sketches at the bottom part of Fig. 3 delineate the side view of what is assumed to be the surface-flow patterns in the two-dimensional area.

In Fig. 3a the bold line indicates approximately where the boundary layer separates. A large portion of the surface flow is in the two-dimensional region except near the wall and tip. In the attached flow area the oil flow moves in the main stream direction. The direction of oil flow is reversed in the separated area while increasing the angle of attack, the location of separation moves toward the upstream direction. The wall effect around the juncture alters the separation pattern, which is comparable with Rizzetta's description for a cylinder/plate juncture.[21] The end effect causes the separation line to curve toward the leading edge. This type of surface-flow pattern exists at low Reynolds numbers and angles of attack and is identified as the regime of separation.

In Fig. 3b two dark lines appear. The left line is where the boundary layer separates, whereas the right one represents where the separated flow reattaches. The direction of oil flow in the two-dimensional region shows the existence of a separation bubble between these two lines, as shown in the bottom part of Fig. 3b. The bubble moves toward the upstream area and becomes smaller with the increase in root angle of attack. This type of surface-flow pattern is identified as the regime of bubble.

In Fig. 3c the separation bubble becomes very small, and both the separation and reattaching lines are located very close to the leading edge. The oil around the leading edge tends to form a characteristic bead-like pattern, which is similar to that observed by Winkelmann and Barlow.[22] A surface vortex[21] appears near the juncture area. This type of surface-flow pattern is identified as the regime of leading-edge bubble.

In Fig. 3d the bubble near the leading edge remains small. The reattached turbulent boundary layer separates and forms a second separation line near the trailing edge. This second separation line moves toward the upstream area with the increase in root angle of attack. This type of surface-flow pattern is identified as the regime of turbulent separation.

In Fig. 3e strong three-dimensional flow effects are observed. Two surface vortices,[21] which is a system of vortices developing

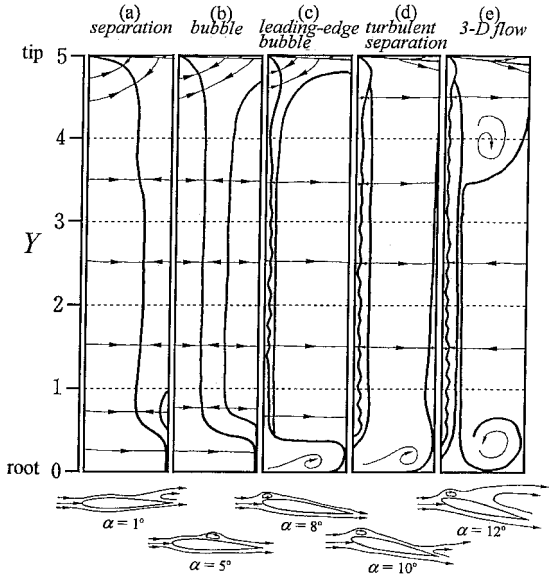

Fig. 3 Hand sketches of typical surface-flow patterns at $T = 0.2\%$, $Re_c = 5.9375 \times 10^4$.

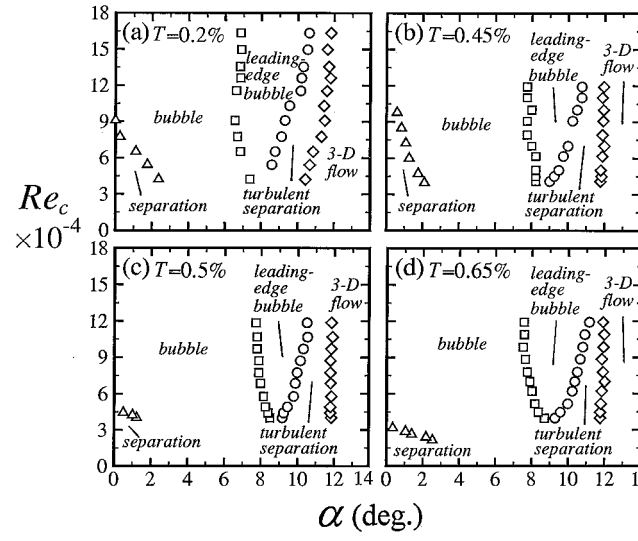

Fig. 4 Characteristic flow regimes.

with vortex filaments not everywhere aligned to the oncoming flow, with one near the root area and the other near the wing tip are generated. The observed three-dimensional separated flow pattern is quite similar to that reported by Bippes[23] and Bippes and Turk.[24] The area occupied by the surface vortex near the tip is much larger than that near the wall. This flow pattern is observed at angles of attack higher than stall and is identified as the regime of three-dimensional flow.

Characteristic Flow Regimes

At nominal freestream turbulence intensity greater than 0.2%, the characteristic surface-flow patterns appear similar to those at $T = 0.2\%$. However, the characteristic regimes of the flows are different, as shown in Fig. 4. The flow regimes are clearly distinguishable except for the boundary between the regimes of bubble and leading-edge bubble. The inception of the leading-edge bubble was artificially judged as the separation line of the bubble that moves upstream from near the midchord to about 3% chord length from the leading edge and stays there without apparent movement with further increase of angle of attack.

The separation is delayed in chord Reynolds number at $T = 0.45\%$, compared with that at $T = 0.2\%$, as shown in Figs. 4a and 4b. However, the separation advances with the increase in turbulence intensity when $T > 0.45\%$ so that the separation regime reduces, as shown in Figs. 4c and 4d. The increase in freestream turbulence intensity enhances the turbulent kinetic energy of the separated shear layer to overcome the adverse pressure gradient. The separated shear layer reattaches to the suction surface and forms a recirculated bubble.[12] The bubble regime extends from about $\alpha = 7$ deg at $T = 0.2\%$ to about 8 deg at $T = 0.45\%$. However, the freestream turbulence intensity has little effect on the formation of bubble (i.e., the occurrence of reattachment) when $T > 0.45\%$, as shown in Figs. 4b–4d. The leading-edge bubble regime extends from about $\alpha = 10$ deg at $T = 0.2\%$ to about 11 deg at $T = 0.45\%$. When $T > 0.45\%$, the leading-edge bubble regime does not change significantly. The critical angle of attack for appearance of the three-dimensional flow pattern increases with the increase in chord Reynolds number at $T = 0.2\%$, as shown in Fig. 4a. When $T > 0.45\%$, the three-dimensional flow pattern appears at $\alpha \approx 11.5$ deg with little increase in Reynolds number, as shown in Figs. 4b–4d.

There exists a critical freestream turbulence intensity, beyond which the regimes of leading-edge bubble, turbulent separation, and three-dimensional flow do not change significantly.

Separation, Reattachment, and Bubble

Figure 5 shows the chordwise locations of separation and reattachment as well as the bubble length varying with angle of attack and chord Reynolds number at $T = 0.2\%$. The chordwise location of

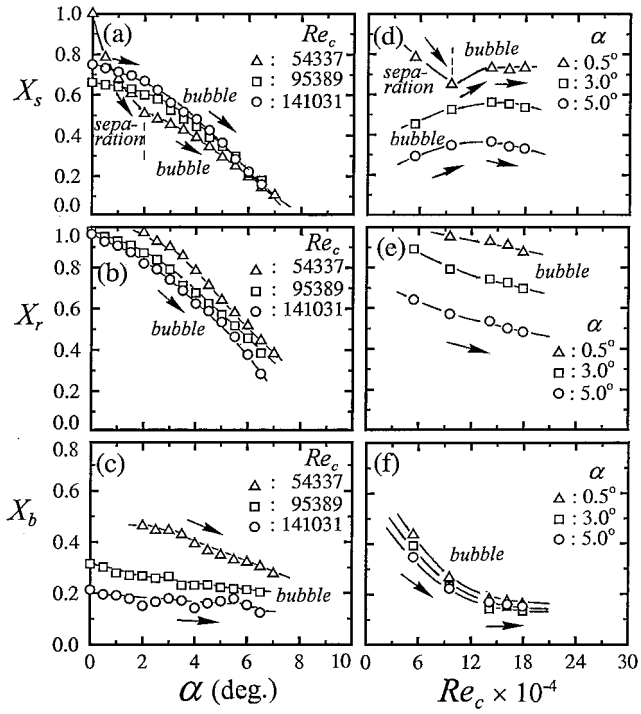

Fig. 5 Typical appearances of separation, reattachment, and bubble length at $T = 0.2\%$.

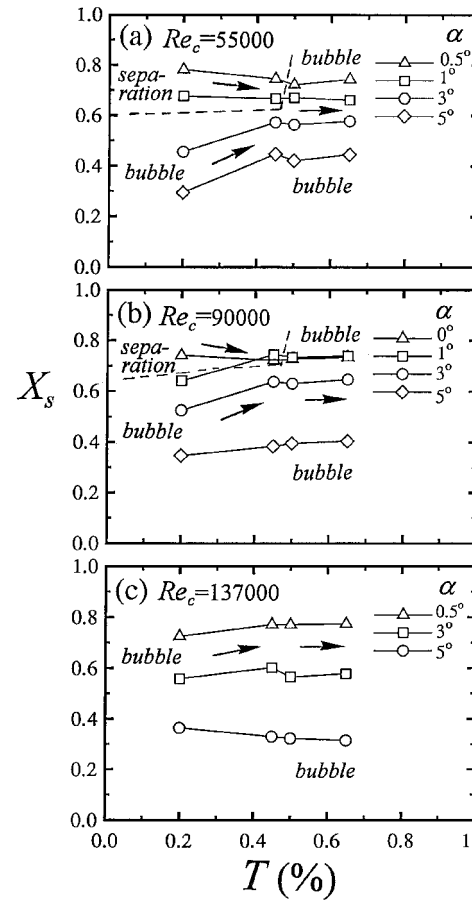

Fig. 6 Variation of separation location with freestream turbulence intensity.

separation in the regime of separation appears quite different from that in the bubble regime. For instance, at $Re_c = 5.4337 \times 10^4$ in Fig. 5a, in the regime of separation the separation occurs around the trailing edge at $\alpha = 0$ deg. The separation occurs around $X_s = 0.5$ at $\alpha = 1.8$ deg. The change rate $\Delta X_s/\Delta\alpha$ is about 0.27/deg. However, in the bubble regime the separation location moves toward the upstream area with a rate $X_s/\Delta\alpha$ about 0.07/deg, which is much smaller than that in the separation regime. The bubble is formed at $\alpha = 0$ deg at Re_c larger than about 9.1×10^4, as shown in Fig. 4a. In the bubble regime, e.g., $Re_c = 9.5389 \times 10^4$ and 1.41031×10^5 in Fig. 5a, the change rate $\Delta X_s/\Delta\alpha$ is small. The separation is found at $X_s \approx 0.7$, and reattachment is observed near the trailing edge at $\alpha = 0$, as shown in Figs. 5a and 5b. Both separation and reattaching lines move toward the upstream area with the increase in α, e.g., about 0.2 and 0.42 chord length from leading edge, respectively, at $\alpha = 6$ deg. The rate of moving forward of the reattaching line is faster than that of the separation line so that the bubble length reduces with the increase in α, as shown in Fig. 5c. For instance, the bubble length reduces from about 47 to 27% chord length as α increases from 2 to 6 deg at $Re_c = 5.4337 \times 10^4$ and from about 32 to 22% chord length as α increases from 0 to 6 deg at $Re_c = 9.5389 \times 10^4$.

At $\alpha = 0.5$ deg, as shown in Fig. 5d, the separation line moves toward the upstream area with the increase in Reynolds number in the separation regime. However, in the bubble regime X_s increases with the increase in Reynolds number for $Re_c < 1.4 \times 10^5$ and decreases slightly for $Re_c > 1.4 \times 10^5$. At $\alpha = 3$ and 5 deg, which are in the bubble regime, the separation lines moves toward the trailing edge with the increase in Reynolds number for $Re_c < 1.4 \times 10^5$ and decreases with the increase in Re_c for $Re_c > 1.4 \times 10^5$. The reattaching lines move toward the leading edge with the increase in Reynolds number, as shown in Fig. 5e. The bubble length shown in Fig. 5f shortens fast with the increase in Reynolds number for $Re_c < 1.4 \times 10^5$. For $Re_c > 1.4 \times 10^5$ the bubble length approaches gradually to about 15% chord length. In general, the bubble length covers about 15–48% of the chord length.

The behavior of the separation, reattaching, and bubble size when $T > 0.45\%$ are similar to those at 0.2% except the locations, change rate, and size. Figure 6 shows the variation of chord-wise location of separation with T. At $Re_c = 5.5 \times 10^4$ as shown in Fig. 6a in the separation region at $\alpha = 0.5$ and 1 deg, the separation locations move upstream with the increase in T when $T < 0.45\%$. When $T > 0.45\%$, the separation locations do not change significantly with the turbulence intensity. However, at $\alpha = 3$ and 5 deg in the bubble regime, the separation locations move downstream with the increase in T when $T < 0.45\%$. When $T > 0.45\%$, the separation locations do not change significantly. At $Re_c = 9 \times 10^4$ as shown in Fig. 6b, the situation is similar except the increase rate $\Delta X_s/\Delta T$, when $T < 0.45\%$ is not as large as that at $Re_c = 5.5 \times 10^4$. At large Reynolds number $Re_c = 1.37 \times 10^5$ as shown in Fig. 6c, the influence of freestream turbulence intensity is not obvious. The effect of freestream turbulence intensity on the separation location is observable only at low Reynolds numbers when $T < 0.45\%$.

Figures 7a–7c show the variation of chord-wise location of reattachment with nominal freestream turbulence intensity at $Re_c = 5.5 \times 10^4$, 9×10^4, and 1.37×10^5, respectively. When $T < 0.45\%$, the reattaching locations in all cases move distinguishably toward the upstream area. When $T > 0.45\%$, the variations of reattaching locations with the increase in T become negligible.

Because the separation location moves downstream and the reattaching location moves upstream with the increase in T when $T < 0.45\%$, as shown in Figs. 6 and 7, the chord-wise length of the bubble decreases drastically with the increase in T when $T < 0.45\%$, as shown in Fig. 8. The reduction of the bubble length with the increase in T at large Reynolds number is less obvious than that at low Reynolds number. Owing to the negligible variations of the separation and reattaching locations when $T > 0.45\%$, as shown in Figs. 6 and 7, the effect of turbulence intensity on the bubble length is not apparent when $T > 0.45\%$, as shown in Fig. 8.

Aerodynamic Performance

Figure 9 shows the lift coefficient C_L, drag coefficient C_D, and lift/drag ratio C_L/C_D, at $T = 0.20\%$. The values of C_L, C_D, and C_L/C_D present distinct slope change in different characteristic

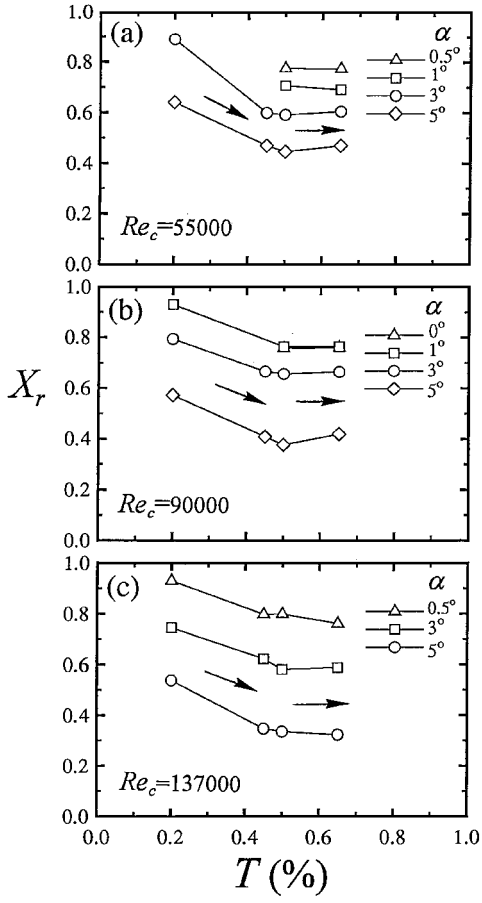

Fig. 7 Variation of reattachment location with freestream turbulence intensity.

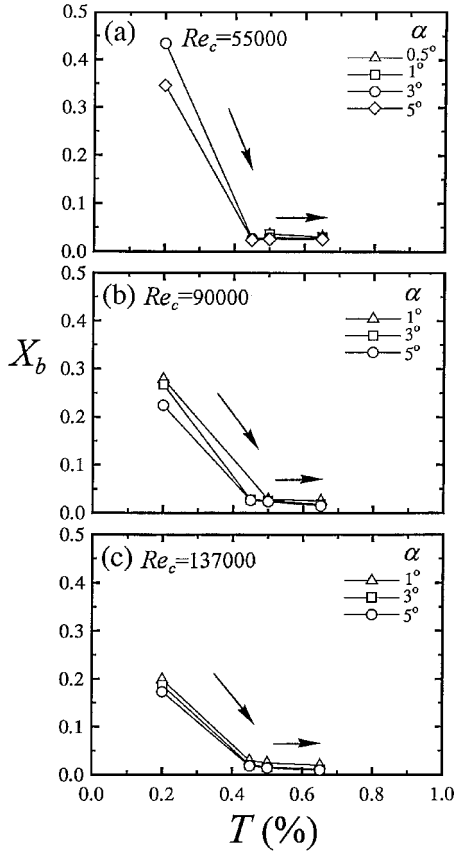

Fig. 8 Variation of bubble length with freestream turbulence intensity.

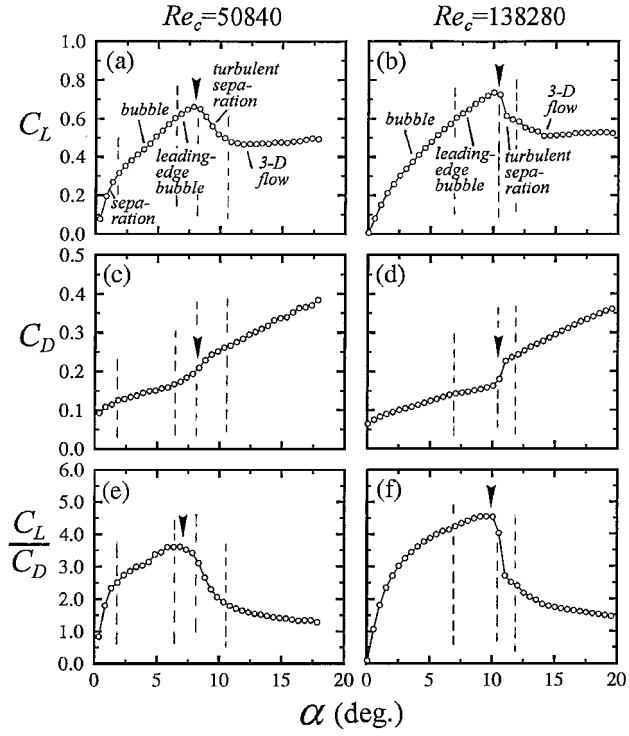

Fig. 9 Typical aerodynamic performance at $T = 0.2\%$.

regimes of surface flows, which are completely different from the conventional result[25] of single-slope value for a Reynolds number larger than 10^6.

As shown in Fig. 9a, the value of lift coefficient increases almost linearly with the angle of attack in the separation regime at $Re_c = 5.084 \times 10^4$. The increase rate $\Delta C_L/\Delta\alpha$ is about $2.08\,\pi$/rad. In the bubble regime the slope of the lift curve reduces to $1.22\,\pi$/rad, which is noticeably smaller than that in the separation regime. The bubble has an apparent negative effect on the lift of wing. The theoretical value obtained from the analytical analysis of a two-dimensional, thin, symmetric flat plate in an inviscid flow is $2\,\pi$/rad (Ref. 26). Abbott and von Doenhoff[25] indicated that for wing sections approximately 12% thick, the lift-curve slope is about 9% greater than its limiting value for thin sections. Hence, the theoretical slope of the lift curve of a 12% thick wing section in an inviscid flow should be about $2.18\,\pi$/rad. The slope of the lift curve in the separation regime is a little less than the theoretical value of the wing section. However, the increase rate in the bubble regime is much less than the theoretical one. The slope of the lift curve in the bubble regime at $Re_c = 1.3828 \times 10^5$, as shown in Fig. 9b, is about $1.36\,\pi$/rad, which is larger than that at $Re_c = 5.084 \times 10^4$. In the leading-edge bubble regime the slopes of lift curves further decrease to 0.70 and $0.86\,\pi$/rad for $Re_c = 5.084 \times 10^4$ and 1.3828×10^5, respectively, as shown in Figs. 9a and 9b. The maximum value of C_L is about 0.661 at $\alpha = 8.35$ deg for $Re_c = 5.084 \times 10^4$ and 0.735 at $\alpha = 10.04$ deg for $Re_c = 1.3828 \times 10^5$. In the regime of turbulent separation, the lift coefficient decreases abruptly to a local minimum within about 1~2 deg angle of attack, as shown in Figs. 9a and 9b. In the three-dimensional flow regime the lift coefficient slightly increases with the increase in angle of attack.

The variations of drag coefficient C_D are shown in Figs. 9c and 9d. The drag increases with the increase in root angle of attack in the regimes of separation, bubble, and leading-edge bubble. The slope of the drag curve increases much at stall when the surface flow is in the regime of turbulent separation. The reattached and separated turbulent boundary layers create a large skin friction on the suction surface,[26] and, accordingly, a large increase in the drag coefficient is observed. The drag coefficient increases almost linearly with the increase in angle of attack in the regime of three-dimensional flow.

The value of C_L/C_D increases from 0.8 to 2.4 almost linearly with the increase in angle of attack in the region of separation,

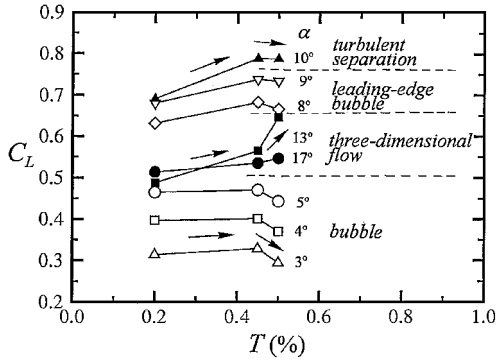

Fig. 10 Influence of freestream turbulence on lift coefficient, $Re_c = 9 \times 10^4$.

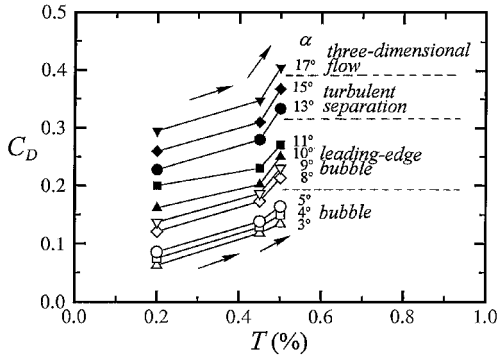

Fig. 11 Influence of freestream turbulence on drag coefficient, $Re_c = 9 \times 10^4$.

as shown in Fig. 9e for $Re_c = 5.084 \times 10^4$. The value of C_L/C_D attains to about 3.6 as turbulent separation starts. The existence of a bubble on the suction surface apparently retards the increase rate of C_L/C_D. In the regime of leading-edge bubble, C_L/C_D drops from 3.6 to 3.4 with the increase in angle of attack because the increase in lift shown in Fig. 9a does not catch up with the rise of drag shown in Fig. 9c. At stall, C_L/C_D decreases fast from 3.4 to 1.8 within only a 2-deg increase in α caused by the abrupt loss of lift. The value of C_L/C_D then decreases slowly with the increase in angle of attack in the three-dimensional flow regime because C_L increases slightly and C_D enlarges rapidly in this regime. The value of C_L/C_D at $Re_c = 1.3828 \times 10^5$ performs better than that at $Re_c = 5.084 \times 10^4$ by comparing Fig. 9f with Fig. 9e.

The variations of C_L with freestream turbulence intensity T at $Re_c = 9 \times 10^4$ are shown in Fig. 10. In the bubble region the lift coefficient C_L increases a little as T increases from 0.2 to 0.45% and then decreases appreciably with the increase in T when $T > 0.45\%$. In the regime of leading-edge bubble, C_L increases to higher values than that in the bubble regime. The lift coefficient increases apparently with the increase in T when $T < 0.45\%$. When $T > 0.45\%$, C_L decreases with the increase in T. The decrease rate is not as large as that in the bubble regime. For $\alpha > 10$ deg, where the wing starts to stall, the lift coefficients drop to low values. In the regime of three-dimensional flow, the lift coefficient increases a little as T increases from 0.2 to 0.45%, which is similar to the behavior in other regimes. However, C_L increases drastically with the increase in T when $T > 0.45\%$.

The variations of C_D with freestream turbulence intensity T at $Re_c = 9 \times 10^4$ are shown in Fig. 11. Drag coefficient increases with both the increases in freestream turbulence intensity in all characteristic surface-flow regimes and the angle of attack. The increase rate $\Delta C_D/\Delta T$ when $T > 0.45\%$ is noticeably larger than that when $T < 0.45\%$. From a conventional point of view, the bubble is largely responsible for the high drag at low Reynolds numbers. Because the large freestream turbulence reduces the bubble size, as has been shown in Fig. 8, one might speculate that reducing the bubble with higher turbulence would lead to less drag. But this is not seen in Fig. 11. Three-dimensional effect might have some contribution to the drag. Although both the lift and drag coefficients increase with increasing freestream turbulence, the value of C_L/C_D still decreases with increasing freestream turbulence intensity, as shown in Fig. 12. In the regimes of bubble, leading-edge bubble, and turbulent separation, the value of C_L/C_D decreases appreciably with the increase in T. The decrease rate is high at large turbulence intensities. In the regime of three-dimensional flow, the influence of turbulence intensity is not particularly obvious.

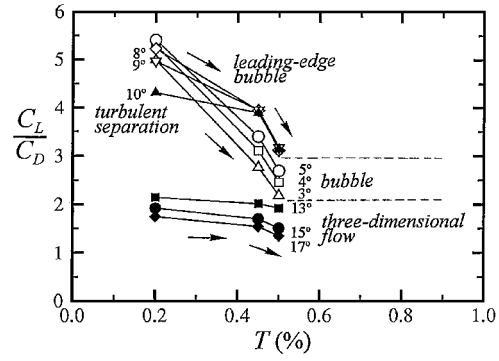

Fig. 12 Influence of freestream turbulence on lift/drag ratio, $Re_c = 9 \times 10^4$.

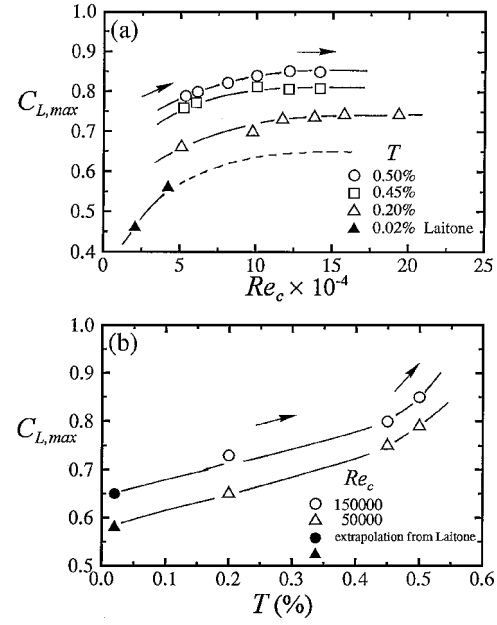

Fig. 13 Variation of maximum lift coefficient with a) Reynolds number and b) freestream turbulence intensity.

Maximum Lift

The variation of maximum C_L with Reynolds number is shown in Fig. 13a. Laitone's experimental results[27] at $T = 0.02\%$, maximum $C_L = 0.46$ at $Re_c = 2.07 \times 10^4$ and maximum $C_L = 0.56$ at $Re_c = 4.21 \times 10^4$, are also shown in the plot for comparison. Laitone's results were obtained from tests of a cantilever wing with an aspect ratio 6. The maximum C_L at $T = 0.2\%$ increases quickly with the increase in Reynolds number for $Re_c < 1.4 \times 10^5$. It attains to about a constant 0.75 for $Re_c > 1.4 \times 10^5$. According to Abbott and von Doenhoff,[25] for an airfoil at Reynolds numbers larger than 10^6 the maximum value of lift coefficient of a NACA 0012 wing section saturates to about a constant 1.60, and the slope of the C_L-α curve is Reynolds-number-independent. The lift of the NACA 0012 wing at low Reynolds numbers performs apparently poorer than

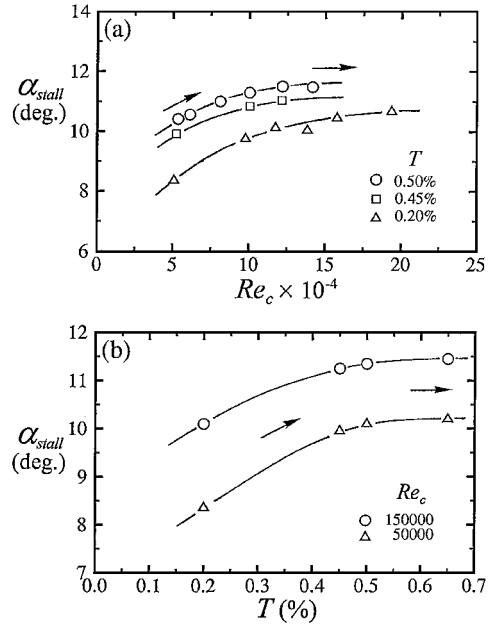

Fig. 14 Variation of angle of attack at stall with a) Reynolds number and b) freestream turbulence intensity.

its counterpart at high Reynolds numbers and even poorer than a thin plate.[27] The maximum C_L at 0.45 and 0.50% freestream turbulence intensities are larger than that at $T = 0.2\%$, which increases with the increase in Reynolds number. The increase rate at each T value retards for $Re_c > 7 \times 10^4$ and approaches, in general, to almost a constant for $Re_c > 1.5 \times 10^5$. At high freestream turbulence intensity, the critical Reynolds number needed to attain constant lift coefficient is lower than that at low freestream turbulence intensity.

The variations of maximum C_L with freestream turbulence intensity at Reynolds numbers $Re_c = 1.5 \times 10^5$ and 0.5×10^5 are shown in Fig. 13b. The maximum lift coefficient increases with the increase in T when $T < 0.45\%$. When $T > 0.45\%$, the increase rate greatens appreciably. The effect of freestream turbulence intensity on the maximum lift coefficient is positive and becomes more obvious when $T > 0.45\%$.

Angle of Attack at Stall

The variation of angle of attack at stall is shown in Fig. 14a. The stall angle of attack at 0.2% freestream turbulence intensity increases from 8.35 deg at $Re_c = 5.084 \times 10^4$ to 10 deg at $Re_c = 1.4 \times 10^5$, then slowly increases to 10.65 deg at $Re_c = 1.95 \times 10^5$. The stall angles of attack at the freestream turbulence intensities of 0.45 and 0.5% are apparently retarded compared with those at $T = 0.2\%$.

The variations of angle of attack at stall α_{stall} with freestream turbulence intensity T at Reynolds numbers $Re_c = 1.5 \times 10^5$ and 0.5×10^5 are shown in Fig. 14b. The angle of attack at stall increases with the increase in T when $T < 0.45\%$. When $T > 0.45\%$, the increase rate retards appreciably and approaches almost constant, e.g., 11.5 deg at $Re_c = 1.5 \times 10^5$ and 10.2 deg at $Re_c = 0.5 \times 10^5$. The high freestream turbulence intensity can effectively delay the stall when $T < 0.45\%$. When $T > 0.45\%$, the influence is insignificant.

Conclusions

The influences of freestream turbulence intensity on the surface-flow regimes and aerodynamic performance are profound. The characteristic regimes of surface flow shift appreciably at different freestream turbulence intensities. With the increase in turbulence intensity, the chordwise location of separation is advanced in the regime of separation and deferred downstream in the bubble regime. The bubble length is significantly shortened with the increase in turbulence intensity. The bubble formed is long (about 15–48%) when $T < 0.45\%$, whereas it is short (about 1–5%) when $T > 0.45\%$.

The aerodynamic loads are strongly correlated with the surface-flow characteristics. The lift and drag coefficients increase almost linearly with angle of attack in the separation regime. The increase rate is much reduced in the regimes of bubble and leading-edge bubble. The stall occurs as turbulent separation appears. The lift coefficient increases with the increase in turbulence intensity when $T < 0.45\%$. However, it decreases with increasing T except in the three-dimensional flow regime. The drag coefficient increases and lift/drag ratio decreases with the increase in freestream turbulence intensity. The effect of freestream turbulence intensity on the maximum lift coefficient is positive and becomes significant when $T > 0.45\%$. The angle of attack at stall increases with the increase in T when $T < 0.45\%$. When $T > 0.45\%$, the increase rate reduces appreciably and approaches almost zero. Large freestream turbulence intensity can effectively delay the stall when $T < 0.45\%$. When $T > 0.45\%$, the influence is not apparent.

Acknowledgments

This study was supported by the National Science Council of the Republic of China under Grant NSC 86-2212-E-011-015.

References

[1]Carmichael, B. H., "Low Reynolds Number Airfoil Survey," Vol. 1, NASA CR 1165803, Feb. 1981.

[2]Crabtree, L. F., "Effect of Leading Edge Separation on Thin Wings in Two-Dimensional Incompressible Flow," *Journal of the Aeronautical Sciences*, Vol. 24, No. 8, 1957, pp. 597–604.

[3]Ward, J. R., "The Behavior and Effects of Laminar Separation Bubbles on Airfoils in Incompressible Flow," *Journal of the Royal Aeronautical Society*, Vol. 67, Dec. 1963, pp. 783–790.

[4]Arena, A. V., and Mueller, T. J., "Laminar Separation, Transition, and Turbulent Reattachment near the Leading Edge of Airfoils," *AIAA Journal*, Vol. 18, No. 7, 1980, pp. 747–753.

[5]Roberts, W. B., "Calculation of Laminar Separation Bubbles and Their Effect on Airfoil Performance," *AIAA Journal*, Vol. 18, No. 1, 1980, pp. 25–31.

[6]Batill, S. M., and Mueller, T. J., "Visualization of Transition in the Flow over an Airfoil Using the Smoke-Wire Technique," *AIAA Journal*, Vol. 19, No. 3, 1981, pp. 340–345.

[7]Mueller, T. J., and Batill, S. M., "Experimental Studies of Separation on a Two-Dimensional Airfoil at Low Reynolds Numbers," *AIAA Journal*, Vol. 20, No. 4, 1982, pp. 457–463.

[8]Pohlen, L. J., and Mueller, T. J., "Boundary Layer Characteristics of the Miley Airfoil at Low Reynolds Numbers," *Journal of Aircraft*, Vol. 21, No. 9, 1984, pp. 658–664.

[9]Mueller, T. J., "The Influence of Laminar Separation and Transition on Low Reynolds Number Airfoil Hysteresis," *Journal of Aircraft*, Vol. 22, No. 9, 1985, pp. 763–770.

[10]Marchman, J. F., "Aerodynamic Testing at Low Reynolds Numbers," *Journal of Aircraft*, Vol. 24, No. 2, 1987, pp. 107–114.

[11]O'Meara, M. M., and Mueller, T. J., "Laminar Separation Bubble Characteristics on an Airfoil at Low Reynolds Numbers," *AIAA Journal*, Vol. 25, No. 8, 1987, pp. 1033–1041.

[12]Hsiao, F.-B., Liu, C.-F., and Tang, Z., "Aerodynamic Performance and Flow Structure Studies of a Low Reynolds Number Airfoil," *AIAA Journal*, Vol. 27, No. 2, 1989, pp. 129–137.

[13]Lissaman, P. B. S., "Low Reynolds Number Airfoils," *Annual Review of Fluid Mechanics*, Vol. 15, 1983, pp. 223–239.

[14]Huang, R. F., Shy, W. W., Lin, S. W., and Hsiao, F.-B., "Influence of Surface Flow on Aerodynamic Loads of a Cantilever Wing," *AIAA Journal*, Vol. 34, No. 3, 1996, pp. 527–532.

[15]Gad-el-Hak, M., "Control of Low-Speed Airfoil Aerodynamics," *AIAA Journal*, Vol. 28, No. 11, 1990, pp. 1537–1552.

[16]Hillier, R., and Cherry, N. J., "The Effects of Stream Turbulence on Separation Bubbles," *Journal of Wind Engineering and Industrial Aerodynamics*, Vol. 8, No. 1–2, 1981, pp. 49–58.

[17]Kiya, M., and Sasaki, K., "Free-Stream Turbulence Effects on a Separation Bubble," *Journal of Wind Engineering and Industrial Aerodynamics*, Vol. 14, No. 1–3, 1983, pp. 375–386.

[18]Mueller, T. J., Pohlen, L. J., Conigliaro, P. E., and Jansen, B. J., Jr., "The Influence of Free-Stream Disturbances on Low Reynolds Number Airfoil Experiments," *Experiments in Fluids*, Vol. 1, No. 1, 1983, pp. 3–14.

[19]Rae, W. H., Jr., and Pope, A., *Low-Speed Wind Tunnel Testing*, Wiley, New York, 1984, pp. 8–40.

[20]Huang, R. F., and Lin, C. L., "Vortex Shedding and Shear-Layer Instability of Wing at Low-Reynolds Numbers," *AIAA Journal*, Vol. 33, No. 8, 1995, pp. 1398–1403.

[21]Rizzetta, D. P., "Numerical Simulation of Turbulent Cylinder Juncture Flowfields," *AIAA Journal*, Vol. 32, No. 6, 1994, pp. 1113–1119.

[22]Winkelmann, A. E., and Barlow, B., "Flowfield Model for Rectangular Planform Wing Beyond Stall," *AIAA Journal*, Vol. 18, No. 8, 1980, pp. 1006–1008.

[23]Bippes, H., "Experimental Investigation of Topological Structure in Three-Dimensional Separated Flow," *Proceedings of the IUTAM Symposium*, Springer–Verlag, Berlin, 1987, pp. 379–381.

[24]Bippes, H., and Turk, M., "Half Model Testing Applied to Wings Above and Below Stall," *Proceedings of IUTAM Symposium*, Springer–Verlag, Berlin, 1990, pp. 22–30.

[25]Abbott, I. H., and Von Doenhoff, A. E., *Theory of Wing Section*, Dover, New York, 1959, pp. 50–53.

[26]Bertin, J. J., and Smith, M. L., *Aerodynamics for Engineers*, Prentice–Hall, Upper Saddle River, NJ, 1989, pp. 150–213.

[27]Laitone, E. V., "Aerodynamic Lift at Reynolds Numbers below 7×10^4," *AIAA Journal*, Vol. 34, No. 9, 1996, pp. 1941, 1942.